JKAU: Eng. Sci., **vol.11 no. 1,** pp. 143-167 (1419 A.H. / 1999 A.D.)

Adaptive Finite-Element Analysis of the Bipolar Ionized Field

Z. AL-HAMOUZ*, M. ABDEL-SALAM* and A. MUFTI*
**Department of Electrical Engineering,*
King Fahd University of Petroleum & Minerals, Dhahran, Saudi Arabia
***Department of Electrical & Computer Engineering*
King Abdulaziz University, Jeddah, Saudi Arabia

ABSTRACT. This paper presents an adaptive finite-element iterative method for the analysis of the ionized field around high-voltage bipolar direct-current (HVDC) transmission line conductors without resort to Deutsch's assumption. Unlike all attempts reported in the literature for the solution of ionized field, the constancy of the conductor's surface field at the corona onset value is directly implemented in the finite-element formulation. The present paper considers both the unequality of the +ve and – ve ion mobility and onset voltage values.

In order to investigate the effectiveness of the proposed method, a laboratory model was built. It has been found that the calculated V-I characteristics and the ground-plane current density agreed well with those measured experimentally. It has been found that taking into account the unequality of +ve and –ve mobility and onset values improved the calculated results towards the experimental values.

1. Introduction

There is an ongoing interest in the analysis of a bipolar ionized field in different geometric configurations. The prospects for the widespread use of HVDC transmission underlie the great interest in the evaluation of corona power loss on bipolar transmission lines[1]. A major difficulty in electrostatic precipitators is the "back corona" which results in a bipolar ionized field that seriously affects the precipitator operation[2]. Bipolar spray charging, as opposed to monopolar charging, was implemented to eliminate corona discharges active at the leaf tips of the crops being sprayed[3].

A Bipolar ionized field includes the generation of positive and negative ions at the coronating conductors and the pertinent recombination between ions of different polarity. This makes the analysis of a bipolar ionized field more complicated than the monopolar one[4].

The equations describing the bipolar ionized field are:

$$\nabla.\vec{E} = (\rho_+ - \rho_-)/\varepsilon_0 \tag{1}$$

$$\vec{J} = k_{\pm}\rho_{\pm}\vec{E} \tag{2}$$

$$\nabla.\vec{J} = \pm R_i\rho_+\rho_- / q_e \tag{3}$$

$$\vec{J} = \vec{J}_+\vec{J}_- \tag{4}$$

$$\nabla.\vec{J} = 0 \tag{5}$$

Equations (1)-(5) are respectively Poisson's equation, the positive and negative current density vectors, $\vec{J}_{\pm}$, the continuity condition of $\vec{J}_{\pm}$, the total current density vector $\vec{J}$ and the continuity condition of $\vec{J}$. k_+ and k_- are the mobilities of positive and negative ions, ρ_+ and ρ_- are the positive and negative space-charge density values. R_i is the ion recombination coefficient in air, and q_e is the electron charge.

The solution of (1)-(5) requires the following boundary conditions:

1) the potentials on the positive and negative coronating conductors are equal to the applied voltages, $+V$ and $-V$, respectively.

2) the potential on the ground plane is zero, and

3) the magnitude of the electric field at the surface of the positive and negative coronating conductors is related to the onset values, E_{crit+} and E_{crit-}, respectively.

4) the potential values of the nodes on the artificial boundary defining the finite element bounded-region are updated and utilized in the finite-element formulation.

The exact solution of (1)-(5) is extremely difficult due to their nonlinear nature. All attempts reported before were based on some simplifying assumptions. The most common ones are:

1) the space is full of charges of both polarities. The thickness of the ionization layer around the conductors is so small as to be neglected with respect to the interelectrode spacing.

2) the space-charge affects only the magnitude and not the direction of the electric field (Deutsch's assumption).

3) the positive and negative ion mobilities k_+ and k_- are constant (independent of field intensity).

4) diffusion of positive and negative ions D_+ and D_- is neglected.

5) the surface field of the coronating conductors remains constant at the onset values E_{crit+} and E_{crit-} irrespective of the corona intensity (Kaptzov's assumption).

6) transmission line conductors are assumed infinite long with negligible sag.

To the authors' knowledge, few attempts have been made to solve the bipolar ionized field equations[1,5-7]. Takuma *et al.*[1,5] applied the finite-element technique (FET) in solving equations (1)-(5) for bipolar configurations. They replaced Kaptzov's assump-

tion with that of constant ion density, namely, the space-charge density is assumed constant around the coronating conductor periphery without justification. Qin *et al.*[6] proposed an iterative charge-simulation technique to solve the bipolar ionized field problem. They adopted the method of weighted residuals in estimating the line charge densities used to simulate the space-charge distribution in the interelectrode spacing. Very recently, Abdel-Salam and Al-Hamouz[7] developed an iterative finite-element technique to solve the bipolar ionized field problem while assuming equal positive and negative ion mobilities and corona onset voltage values. In fact, the positive and negative ion mobilities are different and the corona onset voltage is polarity-dependent.

In the present paper, an adaptive FET is developed for the solution of the bipolar ionized field in HDVC transmission lines. Unlike previous attempts[1,5,6], a new approach of updating the space-charge densities values is adopted in which the positive and negative space-charge density values are estimated by simultaneous integration of a modified form of equation (3) applied for positive and negative space-charge densities. In addition, the unrealistic assumption of equal positive and negative ion mobilities and corona onset voltages adopted in our previous work[7] has been waived. The present method simplifies the computer programming in addition to achieving convergence in small number of iterations.

The triangular finite-element grid is generated from quadrangles produced by the intersection of field lines with equipotential contours[7-10]. In order to satisfy the continuity condition and to estimate the discrete space-charges at the grid nodes, the interelectrode spacing is divided into flux-tubes by field lines. The axis of each flux-tube is also a field line along which the grid nodes are located at the intersections with the equipotential contours. Along these flux-tubes, the ions are driven either from the coronating conductors to the ground plane or from one coronating conductor to the other.

2. Assumptions Adopted by the Proposed Method

Assumption (1) is valid because the ionization layer is of the same order as the conductor's diameter and the latter is negligible in comparison with the spacing between conductors and height above ground plane. Assumption (2) is waived in the present analysis. Assumptions (3) and (4) are retained due to the complications they would introduced if waived. Assumption (5) had been investigated in a previous attempt[11] and was found to be satisfactory especially when the applied voltage is well above the corona onset value.

3. Proposed Method of Analysis

The bipolar configuration investigated consists of two conductors stressed by voltages $+V$ and $-V$, each with a radius R located at a height H above the ground plane and separated by a distance D, Fig. (1). The flow-chart of the proposed method of analysis is shown in Fig. (2). The details of each step of the proposed method are explained below.

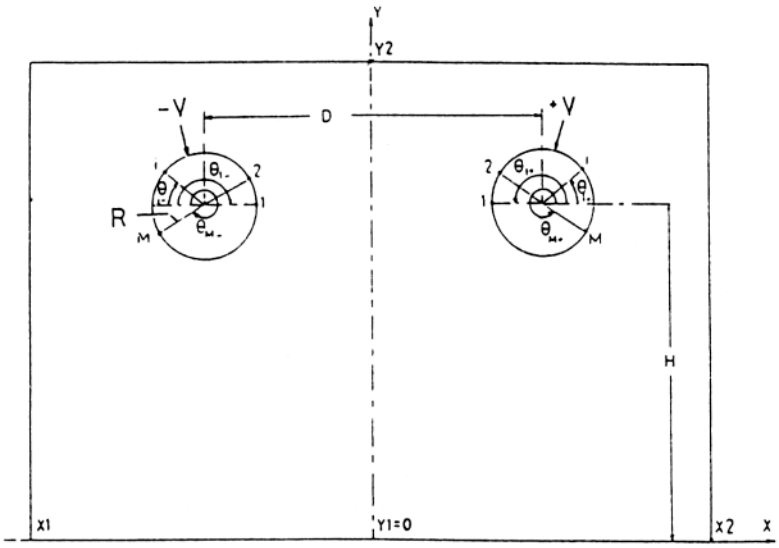

Figure 1. Region where the field lines and equipotential contours are mapped, θ_i, defines the angle at which the i^{th} field line emanates.

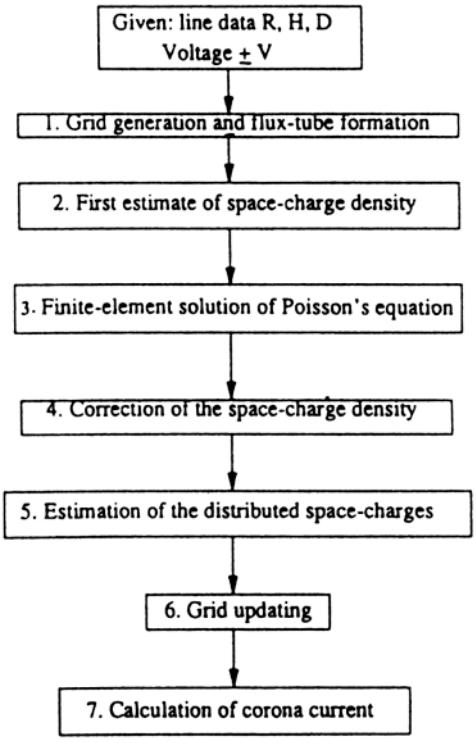

Figure 2. Block diagram of the proposed method of analysis.

Step (1): Grid Generation and Flux-Tube Formation

With the knowledge of the space-charge density values through the interelectrode spacing, the FET is applied to determine the potential and field values and to map the field lines and equipotential contours. Initially, the space-charge density values are not known and, therefore, they are assigned zero. This makes it possible to generate the electrostatic finite-element grid and the flux-tubes along which the ions are driven from one conductor to the other or from conductor to the ground plane.

The electrostatic grid is generated by mapping the space-charge-free field around the bipolar transmission line conductors. Under the applied voltage $\pm V$, the conductors surface charges are simulated[7], by line charges $\pm q$ $(= 2\pi\varepsilon_0 V/\ln(2HD/RK_b)$, where $K_b = \sqrt{(2H)^2 + D^2}$, located at the centers of the conductors. The images of these charges are considered to maintain the ground plane at zero potential.

As the transmission line conductors are assumed infinitely long with negligible sag and the ground plane is assumed horizontal, the investigated configuration is treated as a two-dimensional problem in the $X - Y$ plane.

The field lines are mapped around both transmission line conductors. The field lines emanate from M nodes selected on the circumference of each conductor, Fig. (1). Thus, the total number of field lines in the whole space is $2M$. Each node on the circumference of the positive and negative conductors is located by angle θ_i+ and θ_i–, respectively. It is well known that the finite-element technique calls for bounded region in which the grid is to be generated. The authors succeeded in utilizing the ballooning technique in monopolar-transmission line configurations to move the region bounds to infinity[12]. They found that the choice of the grid fictitious boundaries X1-X2 and Y1-Y2 at 3.5-5.5 times the conductor's height H is satisfactory[12] in the light of the fact that the computed results did not change for larger grid area. Hence, the grid fictitious boundaries X1-X2 and Y1-Y2 are chosen at 7-11 and 3.5-5.5 times the conductor's height for bipolar transmission-line configurations, Fig. (3). The mapped field may be divided into three groups. Group A maps the bipolar ionized-region in which ions of positive and negative polarities convect from one coronating conductor to the other along M_c field lines. On the other hand, groups B and C map the monopolar ionized-regions in which only positive and negative ions convect from the positive and negative coronating conductors to the ground plane respectively. Due to the imposed fictitious boundaries X1-X2 and Y1-Y2, some of the field lines and equipotential contours are not completely mapped, Fig. (3).

The positively and negatively stressed conductor surfaces are equipotentials at their applied voltage values and the ground plane is also equipotential at zero value. Between each conductor equipotential and the ground, N-2 equipotential contours are traced in the monopolar regions B and C, starting close to the conductor. In the bipolar A, there are 2N equipotential contours. Since each transmission line conductor is an equipotential and the zero equipotential contour (which happened to be along the Y-axis midway between the two conductors for the generation of the electrostatic grid only) is to be mapped only once, 2N-3 equipotentials are traced between the two conductors[13]. Along all monopolar/bipolar field-lines which emanate from the surface of the coronating conductors but do

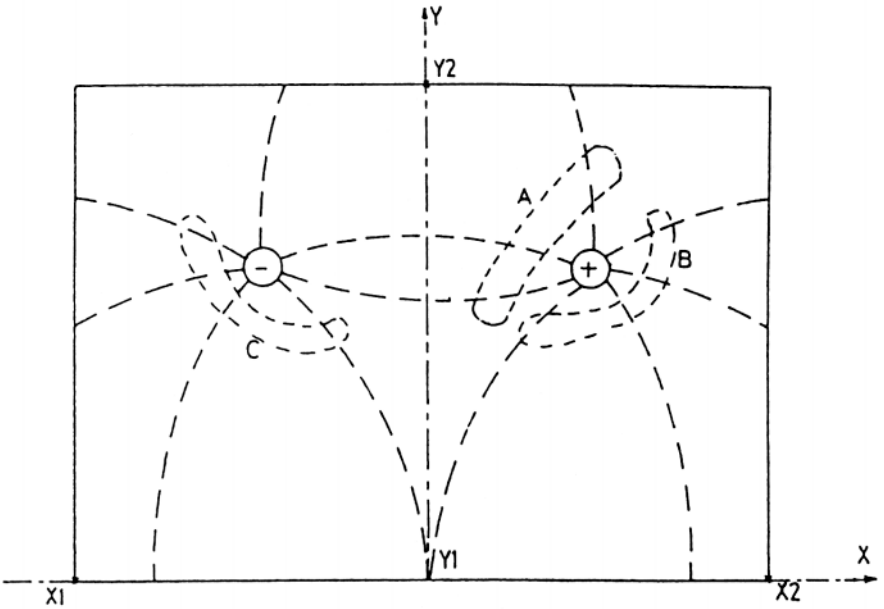

Figure 3. Field lines in monopolar and bipolar regions.

not terminate at the ground plane/opposite conductor, the conductor's surface corresponds to the first equipotential contour and hence represents node #1 along that field line.

The point of intersection between the i^{th} field line and the j^{th} equipotential contour represents the node (i, j) of the proposed grid,[7-10,12,13]. The potential and electric field values $\phi_{i,j}$ and $E_{i,j}$ calculated at the grid nodes are arranged in two-dimensional arrays Φ and E, which are denoted by $\Phi^{(1)}$ and $E^{(1)}$ for the first estimate of the potential and field values. Also, the space-charge densities at these nodes are arranged in two-dimensional arrays, one for the positive space-charge density values ($\rho_{+i,j}$) and the other for negative space-charge density values ($\rho_{-i,j}$).

Step (2) : The First Estimate of the Space-Charge Density

The initial guess of the positive and negative space-charge density located at node (i, 1) around the periphery of the positive and negative conductors, is assumed to follow eqns. (6) and (7)[7,13], respectively:

$$\rho_{+i,1} = \rho_{e+} \cos((\pi - \theta_{i+})/2), \quad i = 1,2,3 \ldots M \tag{6}$$

$$\rho_{-i,1} = \rho_{e-} \cos((\pi - \theta_{i-})/2), \quad i = 1,2,3 \ldots M \tag{7}$$

where the space-charge density is assumed maximum along the line extending between the centers of the coronating conductors and ρ_{e+} and ρ_{e-} are the values of $\rho_{+i,1}$ and $\rho_{-i,1}$ at $\theta_{i\pm} = \pi$. The values of ρ_{e+} and ρ_{e-} were estimated using an approximate expression[7,14] for the charge density at the Y-axis plane as derived in Appendix 1:

$$\rho_{e+} = \frac{E_y D}{E_{crit+} R} 8\varepsilon_0 V_{0+}(V - V_{0+}) / [D^2 V (5 - 4V_{0+}/V)] \tag{8}$$

$$\rho_{e-} = \frac{E_y D}{E_{crit+} R} 8\varepsilon_0 V_{0-}(V - V_{0-}) / [D^2 V (5 - 4V_{0+}/V)] \tag{9}$$

where:

E_y is the pace-charge free field at midway between the positive and negative poles at height H,
E_{crit+} is the corona positive onset field values,
E_{crit-} is the corona negative onset field values, and
V_{0+}, V_{0-} are the corona positive and negative onset voltage values that include the surface roughness factor (η)

Also, initial negative and positive space-charge density values are assumed on the bipolar field lines on the positive and negative conductor surfaces in region A of the ionized field as:

$$\rho_{-i,\,1} = 0.02(\rho_{-i,\,1})_{on\ negative\ conductor} \quad , \quad i = 1,2,3 \ldots M_c \tag{10}$$

$$\rho_{+i,\,1} = 0.02(\rho_{+i,\,1})_{on\ positive\ conductor} \quad , \quad i = 1,2,3 \ldots M_c \tag{11}$$

The initial values of the negative and positive space-charge density expressed by eqns. (10) and (11) are arbitrary chosen equal to 2%. Other choices for these values do not affect the final solution of the problem[13].

To satisfy the positive and negative current continuity conditions along the axis of each flux-tube in the bipolar region A, the current density eqn. (2) is substituted into the current continuity eqn. (3). Rearranging the terms makes it possible to obtain at each node (*i, j*):

$$\frac{d\rho_{+i,j}}{dl} = -\frac{\rho_{+i,j}}{E}\left[R_i \frac{\rho_{-i,j}}{q_e k_+} + \frac{(\rho_{+i,j} - \rho_{-i,j})}{\varepsilon_0}\right. \tag{12}$$

$$\frac{d\rho_{-i,j}}{dl} = \frac{\rho_{-i,j}}{E}\left[R_i \frac{\rho_{+i,j}}{q_e k_-} - \frac{(\rho_{+i,j} - \rho_{-i,j})}{\varepsilon_0}\right. \tag{13}$$

where *l* is the length measured along the axis of the flux-tube starting from the conductors' surface.

Starting at the surface of the positive (or negative) conductor, Fig. 3, simultaneous integration of eqns. (12) and (13) by the fourth order Runge-Kutta method gives the first estimate of the space-charge density values at the nodes along the axis of the flux-tubes in the bipolar ionized region A. For the first step of integration, the value of *E* is taken at E_{crit+} (or E_{crit-}) and the initial space-charge density values are determined from eqns. (6) and (10) if starting at the surface of the positive conductor or eqns. (7) and (11) if starting at the surface of the negative conductor. For the monopolar ionized regions, the space-charge density is determined by integrating eqn. (12) for group-B field lines after setting

ρ_- to 0 and by integrating eqn. (13) for group-C field lines after setting ρ_+ to 0, starting at the surface of the coronating conductor. The initial space-charge density values at the positive and negative conductor surfaces are estimated from equations (6) and (7), respectively.

To calculate the field at node (i, j) along the axis of the i^{th} flux tube in either the bipolar or the monopolar ionized-field regions, a third order interpolating polynomial $f(L)$ of the potentials calculated at nodes $(i, j-1)$, (i, j), $(i, j+1)$ and $(i, j+2)$ has been formulated as before[7, 13]. $f(L)$ is a single-variable polynomial where L is the length measured along the axis of the i^{th} flux-tube starting from the conductor surface to the interpolating node. Taking the derivative of the interpolating polynomial with respect to L at the node of interest, one obtains the magnitude of the electric field at that node.

For all flux-tubes in the monopolar ionized-regions B and C and the flux-tubes in the bipolar ionized-region A which terminate at the fictitious boundaries X1-X2 or Y1-Y2, the field at the node (i, N_f-1) (i.e. node before the last one whose number is N_f) along the i^{th} flux-tube is determined by extrapolating a third order interpolating polynomial formed from the electric field calculated at nodes (i, N_f-5), (i, N_f-4), (i, N_f-3) and (i, N_f-2). However, the field at the last node (i, N_f) is determined from the extrapolation of the third order interpolating polynomial formed from the electric field calculated at nodes (i, N_f-4), (i, N_f-3), (i, N_f-2) and (i, N_f-1).

For the flux-tubes extending between the two coronating conductors, the field at the node $(i, 2N-1)$ (i.e. node before the last one) is determined by extrapolating a third order interpolating polynomial formed from the electric field calculated at nodes $(i, 2N-5)$, $(i, 2N-4)$, $(i, 2N-3)$ and $(i, 2N-2)$. Of course, the field value at the last node $(i, 2N)$ along the field lines extending between the two coronating conductors is the corona onset value, E_{crit-}.

Step (3): Finite-Element Solution of Poisson's Equation

Solving Poisson's equation by the FET calls for division of the region of the mapped field into elements. The quadrangles generated by the intersection of the field lines with the equipotential contours are divided into two triangular elements. In this way, the nodes in the mapped field region constitute the vertices of the elements forming the finite-element grid.

The potential φ within each element is approximated as a linear function of coordinates[15], namely:

$$\varphi = \varphi^e W^e = \varphi_p w_p + \varphi_s w_s + \varphi_t w_t \tag{14}$$

where p, s and t represents the nodes of the element e and W is the corresponding shape function.

To solve Poisson's equation, (1), in the general form, an energy functional $RF^{(e)}$ expressed by eqn. (15) is formulated as the case in the usual FET[15]:

$$RF^{(e)} = -\int_{A_e} [W]^T [(\partial\varphi/\partial x)^2 + (\partial\varphi/\partial y)^2 + (\rho_+ - \rho_-)/\varepsilon_0] dA_e \tag{15}$$

where A_e is the area of the triangular element. [*W*] is the row vector containing the element shape functions and $[W]^T$ is the transpose of *W*.

For known values of ρ_+ and ρ_- at nodes, Poisson's equation is solved by minimizing the energy functional $RF^{(e)}$ with respect to each nodal potential value. This minimization leads to a set of simultaneous equations, for values of φ at nodes, in the form:

$$[k^e]\ [\varphi^e]\ =\ [f^e] \tag{16}$$

where:

- $[k^e]$ is the element stiffness matrix,
- $[\varphi^e]$ is the unknown potentials of the element nodes, and
- $[f^e]$ is the free term which entails the aforementioned boundary conditions and assumed distribution of the charge density ρ at the nodes of the element *e*.

On applying eqn. (16) for all elements of the grid and summing-up the results, the following set of equations is obtained:

$$[K]\ [\Phi]\ =[F] \tag{17}$$

where:

- [*K*] is the global stiffness matrix,
- [Φ] is the vector whose values express the estimated nodal potentials, and
- [*F*] is the assembled free term due to boundary conditions.

The array of nodal potentials is denoted by $\varphi^{(m)}$, representing the potentials in the m^{th} iteration of the solution.

The constancy of the positive and negative conductor surface field values at E_{crit+} and $E_{crit\ -}$ is to be implemented directly into the FE formulation. This is achieved by noting that $(\varphi_{i,\,1} - \varphi_{i,\,2})/\Delta r_i = E_{crit+}$ (or E_{crit-}) where Δr_i is the radial distance between the first two nodes along the axis of any flux tube. The distance Δr_i is chosen much smaller than the radius of the coronating conductor (< 4% of the conductor radius as reported before by Abdel-Salam and Al-Hamouz[16]. Since the potential $\varphi_{i,\,1}$ is the applied voltage (+V) which is known, then $\varphi_{i,\,2}$, the potential at node (*i*, 2), i.e. the i^{th} node along the second equipotential contour is also of known potential.

Due to the nature of the FE grid proposed before[17], being applied only for conductor-to-plane configurations, the procedure for computing the space-charge density at the nodes is complicated and less accurate in comparison with the proposed method of analysis where the nodal space-charge density values are determined directly by simple integration of eqns. (12) and (13) along the axis of the flux-tubes at which the nodes are located.

Step (4): Correction of the Space-Charge Density

Comparing the last two estimates of the potential at the $(i, j)^{th}$ node $\varphi_{i,\,j}^{(m)}$ and $\varphi_{i,\,j}^{(m+1)}$, a nodal potential error e_n relative to the average value φ_{av} of the potential at that node is defined as

$$e_n = |\,\varphi_{i,j}^{(m)} - \varphi_{i,j}^{(m+1)}\,|\,\varphi_{av} \tag{18}$$

where

$$\varphi_{av} = (\varphi_{i,j}^{(m)} + \varphi_{i,j}^{(m+1)}) / 2 \tag{19}$$

If the maximum of e_n along the axis of the i^{th} flux-tube exceeds a pre-specified value, δ_1, correction of the positive and negative space-charge density values at the conductor's surface (corresponding to that i^{th} flux-tube) is made according to the maximum nodal error as in eqn. (20a):

$$\rho_{\pm i,1_{new}} = \rho_{\pm i,1_{old}} [1 + g \max(\varphi_{i,j}^{(m+1)} - \varphi_{i,j}^{(m)} / \varphi_{av}] \quad , \quad i = 1,2,...M_c \tag{20a}$$

where g is an accelerating factor, taken equal 0.5. The error value δ_1 depends on the required accuracy.

Equation (20a) gives the new estimate of the positive and negative charge density values at the first nodes on the positive coronating conductor field lines in the bipolar ionized-region A.

The new estimates of the charge density values at the first nodes on the monopolar ionized-field regions B and C are determined using eqns. (20b) and (20c), respectively.

$$\rho_{\pm i,1_{new}} = \rho_{\pm i,1_{old}} [1 + g \max(\varphi_{i,j}^{(m+1)} - \varphi_{i,j}^{(m)} / \varphi_{av}] \quad , \quad i = M_c + 1,...M \tag{20b}$$

$$\rho_{-i,1_{new}} = \rho_{-i,1_{old}} [1 + g \max(\varphi_{i,j}^{(m+1)} - \varphi_{i,j}^{(m)} / \varphi_{av}] \quad , \quad i = M_c + 1,...M \tag{20c}$$

It is worthy tp mention that the space-charge density values estimated on the positively and negatively stressed poles, eqn. (20), replaced the first estimate made in step (2) by eqns. (6) through (11).

The space-charge density values at the other nodes along each flux-tube are updated by simultaneous integration of eqns. (12) and (13) for the bipolar ionized-region A, and eqn. (12) or (13) for the monopolar ionized-region B or C, to keep the continuity condition of current satisfied. Using the estimated nodal space-charge densities, the FET (step 3) is applied again to obtain a new estimate of the nodal potentials Φ. Iteration of the space-charge correction and potential estimation continues until the maximum value of e_n over all nodes of the FE grid becomes less than the error δ_1.

Step (5): Estimation of Discrete Space-Charges at Grid Nodes

The distributed space-charges are represented by discrete line charges extending parallel to the coronating conductors and located at the grid nodes. Hence, the charge per unit length at node (i, j) is:

$$Q_{i,j} = (\rho_{+i,j} - \rho_{-i,j}) \, v_{i,j} \tag{21}$$

where $v_{i,j}$ is the volume surrounding the node (i, j) per unit length[7-10,12,13,16].

Step (6): Grid Updating

In the next grid generations, the traced field lines and equipotential contours are not

only due to the applied voltage, but also due to the space-charges estimated at the grid nodes in step (5). Also, the recent space-charge density values around the periphery of the coronating conductors, $\rho_{\pm i,\,1}$, i = 1, 2, ... M, evaluated by eqn. (20), are used as initial values when integrating eqns. (12) and (13).

Steps (1-6) are repeated until the maximum mismatch in the nodal space-charge density values between two successive grid generations is less than a pre-specified error δ_2.

Step (7): Calculation of Corona Current

For each applied voltage above the onset value, the total corona current on the corresponding transmission-line conductor is equal to the sum of the currents flowing in M flux-tubes around its circumference, i.e.:

$$I = \sum_{i=1}^{M} J_i S_{i,1} \tag{22}$$

or

$$I = \sum_{i=1}^{M} (J_{i+} + J_{i-}) S_{i,1} \tag{23}$$

where $S_{i,\,1}$ is the per-unit length cross-sectional area of the i^{th} flux-tube at the conductors surface, and J_{i+} and J_{i-} are respectively the current density values at the positively- and negatively-stressed conductor.

Thus, for the investigated bipolar transmission line configuration, the corona current per unit length of the transmission line is expressed by eqns. (24) and (25) for the positively- and negatively-stressed conductor

$$I_+ = \left(\sum_{i=1}^{M} k_+ \rho_{+i,1} + \sum_{i=1}^{M_c} k_- \rho_{-i,1} \right) E_{crit+} S_{i,1} \tag{24}$$

$$I_- = \left(\sum_{i=1}^{M} k_- \rho_{-i,1} + \sum_{i=1}^{M_c} k_+ \rho_{+i,1} \right) E_{crit-} S_{i,1} \tag{25}$$

where M_c is the number of bipolar field lines along which ions convect from one conductor to the other.

4. Experimental Set-Up and Procedure

Experimental work was carried out at the high voltage laboratory of King Abdulaziz University. Figure (4) shows a plan-view and a picture of the designed experimental set-up which consists of:

1) a grounded aluminum plate to simulate the ground-plane,
2) two parallel conductors which represent the transmission line stretched between isolating vertical supports,
3) two high voltage (HV) d.c. sources (one to generate positive voltage and the other to generate negative voltage) for stressing the transmission line conductors,

4) three microammeters A1, A2 and A3 for measuring the corona current and the ground-plane current density.

The ground plate, $3.6 \times 2.44\ m^2$ in dimension, was made of aluminum sheet, 1 mm in thickness. To maintain the aluminum plate horizontally, it was fixed to a wooden plate of the same size at 0.50 m above the concrete floor. In order to measure the current density distribution underneath the transmission line conductors, the aluminum plate was divided into 69 strips, each of $2.44 \times 0.05\ m^2$ and separated from each other by a distance of 1 mm. Each strip is grounded through the microammeter A3 to measure the corona current received by this strip. With the aid of a panel, Fig. (4), placed in the control room outside the laboratory, the microammeter A3 can serve in measuring the current flowing in all strips by switching it from strip to strip.

Transmission line conductors of two diameters (3.1 mm and 2 mm) are tested. In order to vary the transmission line height above the grounded plate, the height of the insulating supports was made variable. In addition, to vary the conductors' spacing, the insulating supports were made to slide on insulating bases. The two ends of each transmission line conductor are terminated by spherical caps in order to prevent corona from taking place at these ends.

To keep the HV current connection free from corona, the HV sources are connected to the corresponding transmission line through microammeters A1 and A2 using thick aluminum bars (10 mm diameter). As can be seen in Fig. (4), microammeters A1 and A2 are housed in spherical metallic cages to maintain them free from corona by preventing the meter from being exposed to the high electric field.

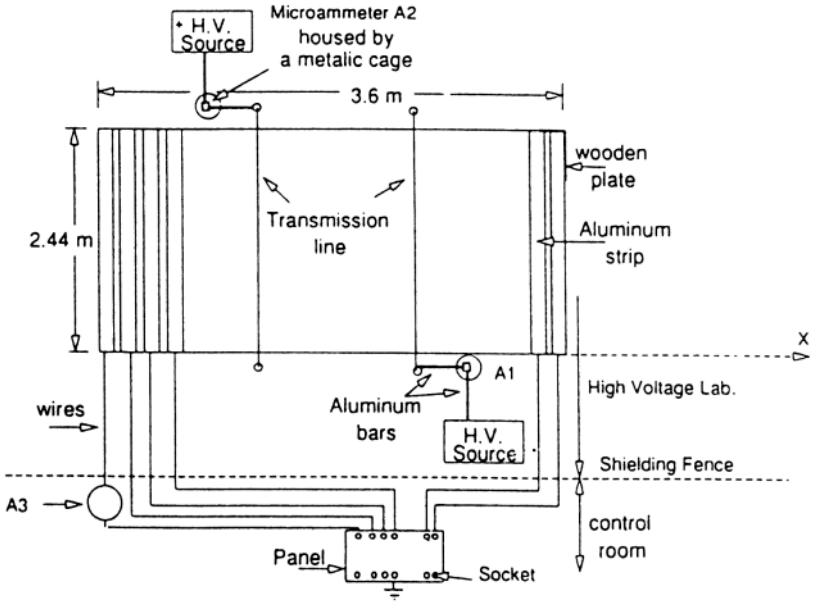

Figure 4. Experimental set-up: (a) plan-view.

1 – + Ve HV source
2 – — Ve HV source
3 – Cage
4 – Microammeter Al
5 – Isolating supports
6 – Spherical cap
7 – T.L. conductor
8 – Aluminum bar
9 – Aluminum grounded plate

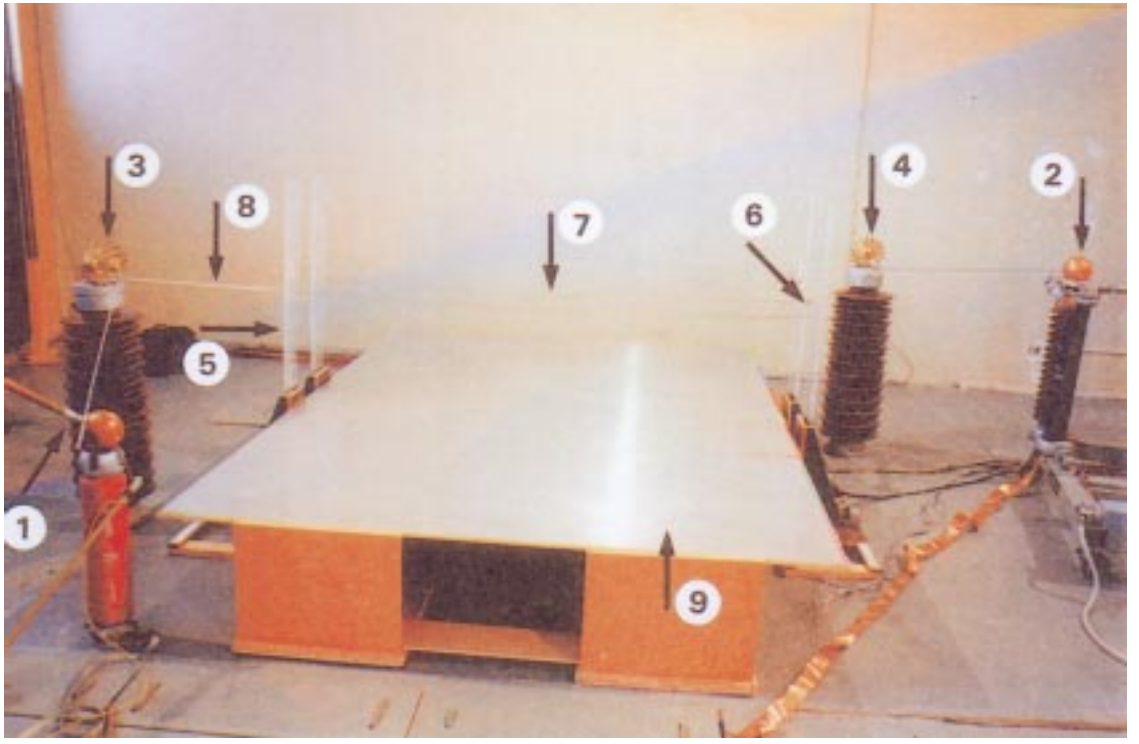

Figure 4b. Picture (At KAU High Voltage Laboratory).

For a specified transmission line conductors each with radius R located at height H above the grounded plate and separated by a distance D, the applied positive and negative voltage are increased simultaneously from zero and the reading of microammeters A1 and A2 is watched. When either of the microammeters starts reading, the corresponding applied voltage is the corona onset value. For different applied voltages above the corona onset value, the corona current is recorded to predict the V-I characteristics for this line configuration at different heights above the ground plane.

For an applied voltage above the corona onset value, the current-density profile at the ground plane is obtained by measuring how the current changes from strip to strip on the grounded plate. Plots of the strip current-density versus the x-coordinate of the strip underneath the transmission line gives the required current-density profile.

5. Results and Discussion

Different bipolar transmission line configurations were tested in the laboratory. Smooth conductors ($\eta = 1$) with radii's 1 mm and 1.55 mm were tested with heights of 0.29 m and 0.545 m above the ground plane and spacings of 0.45 m and 0.6 m. The positive and negative ion mobilities were taken as $1.5 \times 10^{-4}\ m^{2}/Vs$ and $1.7 \times 10^{-4}\ m^{2}/Vs$, respectively. The recombination coefficient R_i was taken as $2 \times 10^{-12}\ m^3/s$[18] and the errors δ_1 and δ_2 were assumed 0.5% in the present analysis.

5.1 V-I Characteristics

For different tested configurations, the present method converges[13] in 3 grid generations with 4-5 iterations in each. This is less than in the case of monopolar ionized field analyzed by Abdel-Salam and Al-Hamouz[10] where 6-7 iterations in each grid generation are required. This is simply attributed to the effect of recombination in reducing the space-charge density in the interelectrode spacing with a subsequent rapid convergence to the required solution.

The V-I characteristics measured and calculated by the proposed method for two different transmission-line configurations are shown in Fig. (5). The agreement between the measured and calculated results is satisfactory. It is quite clear that the value of the corona current of the negative conductor is higher than that of the positive one. This is due to the fact that corona starts on the negative conductor earlier than on the positive conductor since its corona onset voltage is lower than that of the positive conductor value. This is in addition to the higher mobility of negative ions.

For conductor radius of 1 mm, the effects of varying the conductors' height and spacing on the measured and calculated V-I characteristics are shown in Figs. (6) and (7), respectively. The higher the conductors' height above the ground plane, the smaller is the corona current for the same applied voltage. This is simply explained by the corresponding decrease of the electric field along the flux-tubes where the ions are driven between the conductors in the bipolar region A or between the conductors and the ground plane in the monopolar regions B and C. Such a decrease of the field reflects itself on a lower current density along the flux-tubes and hence lower corona current with the increase of

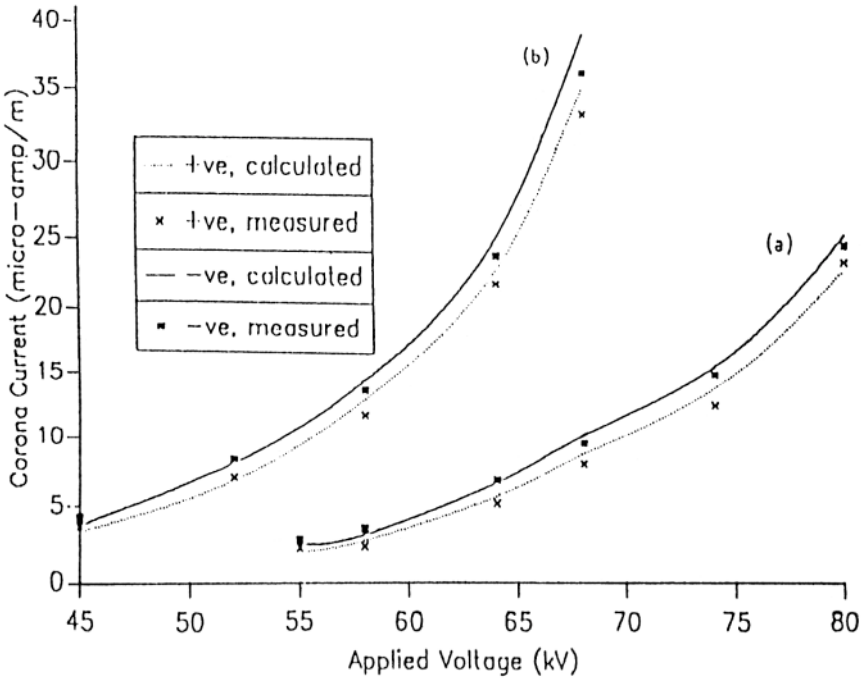

Figure 5. Calculated and measured positive and negative V-I characteristics of two transmission-line configurations ($\eta = 1$).
(a) $H = 0.545\ m$, $D = 0.6\ m$, $R = 0.00155\ m$, $\eta = 1$
(b) $H = 0.29\ m$, $D = 0.45\ m$, $R = 0.001\ m$, $\eta = 1$

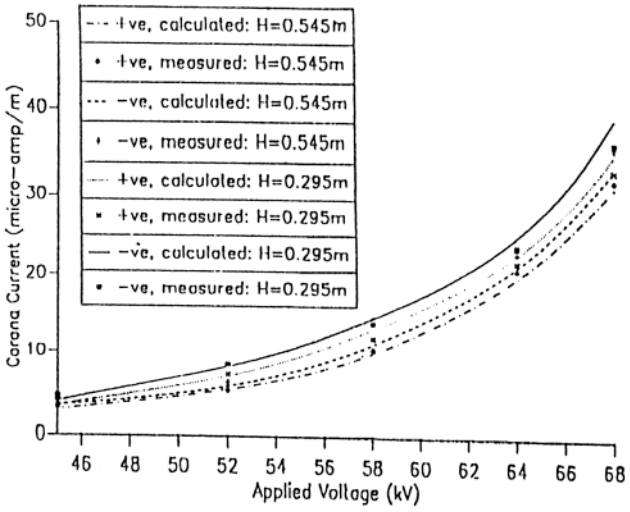

Figure 6. Effect of the conductor's height on the positive and negative V-I characteristics measured and calculated by the proposed method for a bipolar transmission line configuration ($R = 0.001\ m$, $D = 0.45\ m$, $\eta = 1$).

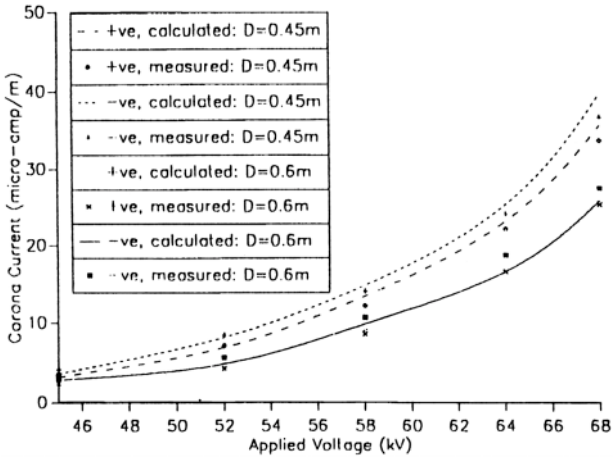

Figure 7. Effect of the conductor's spacing on the positive and negative, V-I characteristics measured and calculated by the proposed method for a bipolar transmission line configuration (R = 0.001 m, H = 0.295 m, η = 1).

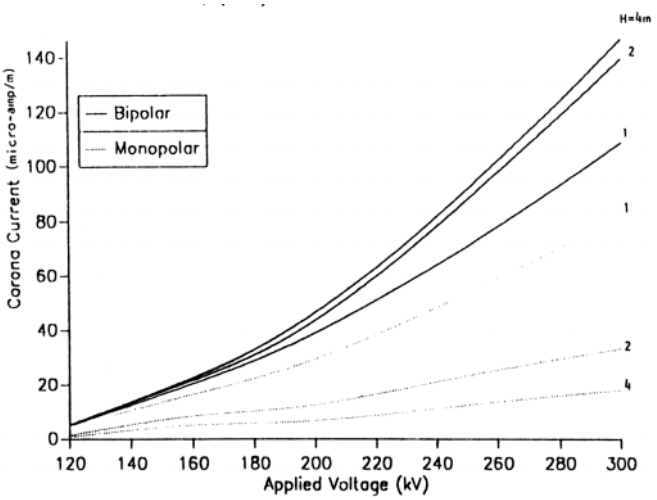

Figure 8. Effect of the conductor's height on the monopolar and bipolar components of the corona current (D = 3 m, R = 0.0025 m, η = 1).

the conductor's height, Fig. (6). However, the corona current components, bipolar and monopolar, change differently. The bipolar component, which is the dominant component of the corona current, increases while the monopolar component decreases with the increase of the conductors' height, Fig. (8). This agrees with the previous findings[14].

The larger the spacing between conductors, the smaller is the recombination between positive and negative ions in the bipolar region A. This reflects itself in increasing the screening action of the positive and negative space-charges around the respective coronat-

ing conductor resulting in a reduction of the field in the conductor vicinity. Subsequently, the corona current convected along flux-tubes in the bipolar region decreases with the increase of the spacing between conductors for the same applied voltage. As the bipolar component is the dominant component of the corona current, the latter decreases with the increase of conductors' spacing for the same applied voltage as shown in Fig. (7).

Also, the conductor's radius affects the measured and calculated V-I characteristics for the same conductor height and spacing as shown in Fig. (9). The smaller the conductors' radius, the lower is the corona onset voltage with a subsequent increase of the corona current for the same applied voltage as depicted in Fig. (9). As regards the computed V-I characteristics, they agree satisfactorily with those measured experimentally, Figs. (6), (7) and (9).

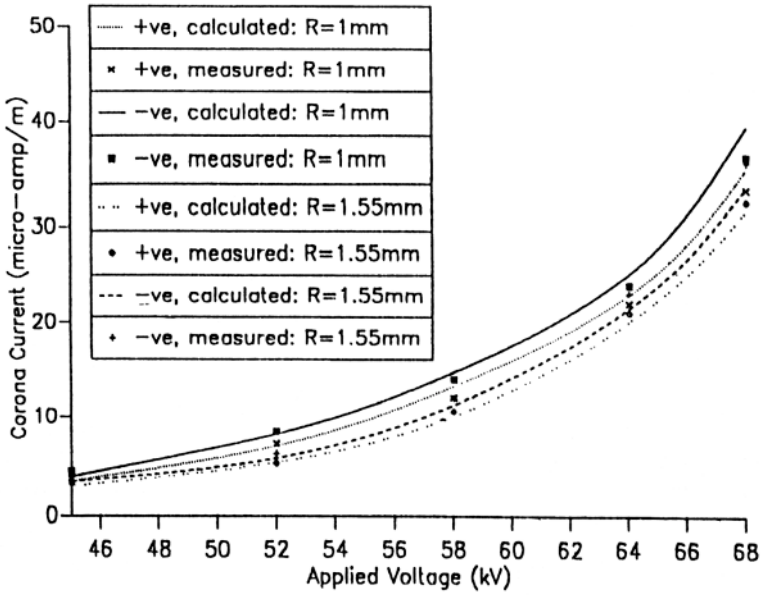

Figure 9. Effect of the conductor's radii on the positive and negative V-I characteristics measured and calculated by the proposed method for a bipolar transmission line configuration (H = 0.295 m, D = 0.45 m, (η = 1).

It is worthy to mention that the proposed algorithm predicts also the V-I characteristics for full-scale transmission lines and the results agreed satisfactorily with previous calculated values[19], Fig. (10). It appears the unequal positive and negative onset-voltage and ion-mobility values improve the calculated results by about 5% in comparison with the case if they are assumed equal as reported by the authors[7].

5.2 Corona power loss

With the knowledge of the V-I characteristics for the transmission line configuration of Fig. (5), the corona power loss in kW/km is determined which increases nonlinearly

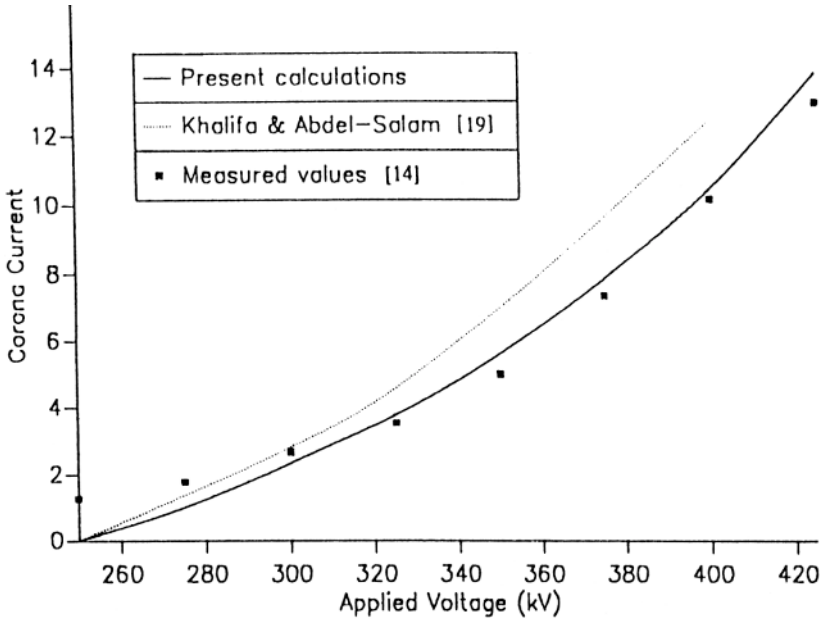

Figure 10. Calculated V-I characteristics of a full-scale bipolar transmission line configuration as compared to previous measured and calculated values (H = 9.15 m, D = 10.36 m, R = 0.0102 m, η = 0.7).

with the applied voltage. It is worthy to mention that, when the line operates at full capacity, the corona power loss as a percentage of the ohmic power loss is very low (2.5%) when the applied voltage is very close to the corona onset value and reaches about 100% at an applied voltage equal to twice the onset value. Moreover, these percentages can assume higher values if the transmission line is slightly loaded[13].

5.3 Current-density profiles at the ground plane

For different bipolar transmission line configurations tested in the laboratory, the measured and calculated current density profiles at the ground plane are shown in Fig. (11). It is clear that the agreement between the measured and calculated values is satisfactory. The deviation between the measured and calculated values can be attributed to some experimental errors.

For the same applied voltage, the effect of varying the conductors spacing, D, on the ground-plane current density profile is depicted in Figs. (11a) and (11b) at constant conductors' height and radius. On the other hand, the effect of varying the conductors' height, when all other parameters are fixed, on the ground-plane current-density profile is shown in Figs. (11a) and (11c). It is interesting to observe the higher current values underneath the negative conductor with respect to those underneath the positive conduc-

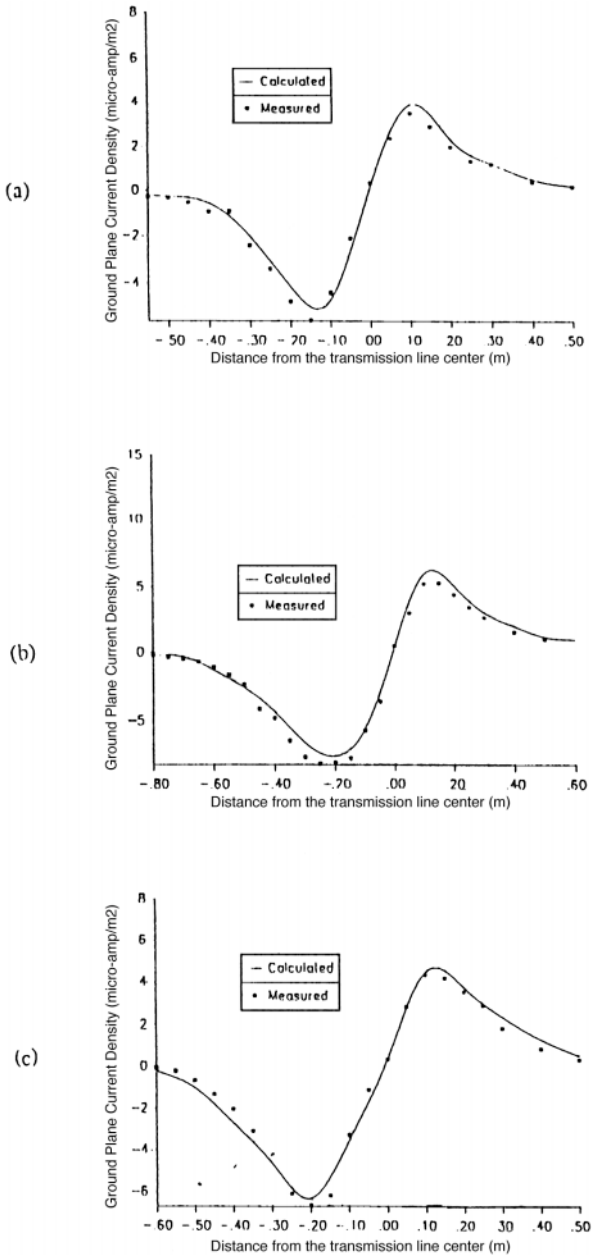

Figure 11. Distribution of the current density profiles at the ground-plane measured and calculated by the proposed method for a bipolar transmission line configuration (V = 68kV, R = 0.00155 m, η = 1).
(a) H = 0.295 m, D = 0.6 m
(b) H = 0.545 m, D = 0.45 m
(c) H = 0.295 m, D = 0. 45 m

tor. This has already been ascribed to the lower onset-voltage and the higher ion-mobility for the negative polarity in comparison with those for the positive polarity.

It is worthy to mention that the approximate expressions of eqns. (8) and (9), which is used as an initial guess for estimating the space-charge around the conductor surface, has a unique value for each transmission line configuration. As expressed in eqns. (10) and (11), the initial value of the negative and positive space-charge density values at the corresponding positive and negative conductors are arbitrary chosen equal to 2% of the positive and negative space-charge values. It is found that other choices of this percentage do not affect the finial solution of the problem, but affects the number of iterations required for convergence[7,13].

5.4 Accuracy, simplicity and computational time

It is quite clear that the calculated values predicted by the proposed adaptive finite-element method are in good agreement with the present and previous measured and calculated values, Figs. (5)-(11).

Also, it is worthy to state that the present method implements directly both the potentials at the coronating conductors and the ground plane and the electric field values at the coronating conductors' surface as boundary conditions in the FE formulation, as proposed before by the same authors[7-10,12,13,16]. However, the previous methods [1,5,6,14,17] deal only with the potentials of the coronating conductors and the ground plane and check later the value of the surface electric field.

Also, the previous methods[1,5,6,14,17] call in their programming for two inner loops to guarantee convergence, one for the convergence of the potential and the other for the convergence of the electric field values. An outer loop to update the mapped field lines (i.e. the FE grid) is also required which means that a total of three loops is needed for convergence of the previous methods[1,5,6,14,17]. On the other hand, the proposed method requires only one loop to guarantee the convergence of the potential, and one loop to update the generated grid. Hence a total of two loops is needed to guarantee convergence.

The number of iterations required for convergence of the solution for the laboratory tested configurations are shown in Table (1).

As our method is applied only to bipolar transmission line configurations with single conductors, comparison with previous attempts[1,5,6] was not possible since they were applied to lines with bundle conductors.

6. Conclusions

An adaptive iterative finite-element based method is developed for the computation of the ionized field in bipolar HVDC transmission lines. Unlike all attempts reported in the literature, the constancy of the electric field at the conductor surface is implemented directly in the finite-element formulation. In addition, the method of analysis make it possible to account for the inequality of the positive and negative ion mobilities and onset voltages.

Table 1. Total number of iteration required for convergence for the tested bipolar transmission line configuration.

Configuration			Number of iterations
H (m)	R (mm)	D (m)	
0.29	1	0.45	12
		0.6	12
	1.55	0.45	12
		0.6	12
0.545	1	0.45	12
		0.6	15
	1.55	0.45	15
		0.6	15

The effect of conductors' height above the ground-plane on the total corona current as well as its monopolar and bipolar components has been investigated. The total corona current decreases with the increase of the conductors' height. On the other hand, the bipolar component increases while the monopolar component decreases with the increase of the conductors' height. Also, the effect of the conductors' spacing and radius has been investigated. The corona current decreases with the increase in the conductors' spacing and increases with the decrease in the conductors' radius.

The number of iterations required to achieve convergence is less than the monopolar case due to the effect of recombination in reducing the space-charge density in the interelectrode spacing. Hence, the present method is characterized not only by its quick convergence, but also by low number of iterations and simplicity in computer programming.

References

[1] **T. Takuma, T. Ikeda** and **T. Kawamoto, "**Calculation of ion flow fields of HVDC transmission lines by the finite element method", *IEEE Trans. Power Appar. Sys.*, Vol. **100,** pp. 4802-4810, 1981.

[2] **P. Levin** and **J. Hoburg, "** Doner cell-finite element descriptions of wire-duct precipitator fields, charges and efficiencies", *IEEE Trans. Ind. Appl.*, Vol. **26,** pp. 662-670, 1990.

[3] **S. Cooper** and **E. Law,** "Bipolar spray charging for leaf-tip corona reduction by space-charge control", *IEEE Trans. Ind. Appl.*, Vol. **23,** pp. 217-223, 1987.

[4] **M. Abdel-Salam,** *Electric Fields in High Voltage Engineering – Theory and Practice*, ed. **M. Khalifa**, (New York-Marcel Dekker), 1990.

[5] **T. Takuma,** and **T. Kawamoto,** "A very stable calculation method for ion flow field of HVDC transmission lines", *IEEE Trans. Power Delivery*, Vol. **2,** 189-198, 1987.

[6] **B. Qin, J. Sheng, Z. Yan,** and **G. Gela, "**Accurate calculation of ion flow field under HDVC bipolar transmission lines", *IEEE Trans. Power Delivery*, Vol. **3,** pp. 368-376, 1988.

[7] **M. Abdel-Salam** and **Z. Al-Hamouz,** "A finite-element analysis of bipolar ionized field", *IEEE Trans. Ind. Appl.*, Vol. **31**, pp. 477-483, 1995.

[8] **M. Abdel-Salam** and **Z. Al-Hamouz,** "Analysis of the monopolar ionized field as influenced by ion diffusion", *Proc. IEEE-IA Annual Meeting, Toronto*, pp. 1817-1822, 1993.

[9] **M. Abdel-Salam,** and **Z. Al-Hamouz,** "A novel finite-element analysis of space-charge modified fields". in press, *Proc. IEE Pt. A* , 1994.

[10] **M. Abdel-Salam** and **Z. Al-Hamouz, "**Finite-element analysis of monopolar ionized field including ion diffusion", *J. Phys D: Appl. Phys.*, Vol. **26,** 2202-2211, 1993.
[11] **M. Khalifa** and **M. Abdel-Salam,** "Calculating the surface fields of conductors in corona", *Proc. IEE*, Vol. **120,** 1574-1575, 1973.
[12] **A. Mufti, Z. Al-Hamouz** and **M. Abdel-Salam, "**Adaptive finite-element ballooning analysis of monopolar ionized field", *Journal of King Abdulaziz University, Engineering Sciences*, 1996.
[13] **Z. Al-Hamouz,** *Analysis of the Ionized Field Around HVDC Transmission Lines*, Ph.D. Dissertation, Dept. of Electrical Engineering, King Fahd University of Petroleum & Minerals, Saudi Arabia, June, 1994.
[14] **M. Sarma** and **W. Janischewskyj, "**Analysis of corona losses on dc transmission lines Pt. II – Bipolar lines", *IEEE Trans. Power Appar. Sys.*, Vol. **88,** pp. 1476-1491, 1969.
[15] **L. Segerlind,** *Applied Finite Element Analysis*, (New York, John Wiley & Sons), 1984.
[16] **M. Abdel-Salam** and **Z. Al-Hamouz, "**A new finite-element analysis of an ionized field in coaxial cylindrical geometry", *J. Phys D: Appl. Phys.*, Vol. **25,** pp. 1551-1555, 1992.
[17] **J.L. Davis** and **J.F. Hoburg,** "HVDC transmission line computations using finite element and characteristics method", *J. Electrostat.*, Vol. **18,** pp. 1-22, 1986.
[18] **S. Brown,** *Basic data of plasma physics*, (New York, John Wiley & Sons) 1966.
[19] **M. Khalifa** and **M. Abdel-Salam,** "Improved method for Calculating DC corona losses", *IEEE Trans.*, Vol. **93,** pp. 720-726, 1974.
[20] **J. Simpson** and **A. Morse, "**Corona on direct-current transmission lines", *Bull. Radio and Elec. Engrg. Div, Nall. Res. Council Canada*, Vol. **14,** pp. 18-30, 1964.

Appendix 1
Initial estimation of ρ_e at the conductor's surface

A rough estimate of the space-charge density at nodes e and e', Fig. (A1), on the surface of the coronating conductor is derived in this Appendix. Assuming completely symmetrical bipolar transmission line configuration where the positive and negative corona onset voltage values V_{0+} and $V_{0\_}$ and the positive and negative ion mobilities K_+ and $K_\_$ are equal implies that the midway equipotential along the y-axis is always of zero potential, hence a rough estimate to the space-charge density value at the point *C*, midway along the axis e-e' is obtained as follows[14]. Consider the coaxial cylindrical configuration formed by placing a cylinder of diameter D concentric with the actual conductor as shown in Fig. (A1), the corona current for voltages just above the corona onset values is given[20] by

$$I = 32\pi\varepsilon_0 k V_0 (V - V_0)/[D^2 \ln(D/2R] \qquad (A\text{-}1)$$

The current density at the surface of the outer cylinder is given as

$$j = k\rho_c E = k\rho_c \zeta\xi = k\rho_c \zeta 2V/[D^2 \ln(D/2R)] \qquad (A\text{-}2)$$

where ξ and ζ are the space-charge free field and a scalar function of the space coordinates that related the space-charge field with the free space-charge one, respectively. In addition (A-2), ζ is approximated by

$$\zeta = 5 - 4(V_0/V) \qquad (A\text{-}3)$$

where the approximation of eqn. (A-3) has been made after getting many iterative solutions of the ionized field along the axis e-e' and having a general nature of ζ.

Using equation (A-3), the total corona current in terms of the current density given in eqn. (A-2) is therefore obtained as

$$I = \pi Dj = 2\pi k\rho_c\left(5 - 4\frac{V_0}{V}\right)V/[D\ln(D/2R) \qquad (A\text{-}4)$$

Comparing eqns (A-1) and (A-4), the approximate value of the charge-density at the outer cylinder is obtained as

$$\rho_c = 16\varepsilon_0 V_0(V - V_0)/[D^2V(5 - 4V_0/V)] \qquad (A\text{-}5)$$

The estimate of the space-charge density at point e on the surface of the coronating conductor is obtained by applying the current continuity equation along the tube T. This implies that

$$k_e\rho_e E_e A_e = k_c\rho_c E_c A_c \qquad (A\text{-}6)$$

or, for constant k

$$\rho_e = \rho_c \frac{E_c A_c}{E_e A_e} \qquad (A\text{-}7)$$

but for the coaxial cylindrical configuration of Fig. (A-1), $Ac = \frac{D}{2}\theta$ and $A_e = R\theta$, hence eqn. (A-7) becomes

$$\rho_c = \frac{DE_c}{2RE_e} \qquad (A\text{-}8)$$

but E_e, the field value at the conductor's surface, equals $E_{0\pm}$, and E_c is assumed equal to the space-charge free field, E_y, at the point midway along the e-e' axis at height H. Hence, substituting eqn. (A-5) into eqn. (A-8) yields:

$$\rho_e = \frac{E_y D}{E_{0\pm}R} 8\varepsilon_0 V_0(V - V_0)/[D^2V(5 - 4V_0/V)] \qquad (A\text{-}9)$$

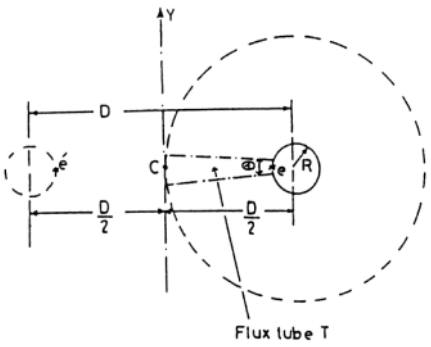

Figure A-1. Pertaining to calculation of approximate value of ρ_e.

Acknowledgements

The authors would like to thank their respective universities for the support they received during the progress of this work.

تحليـل متكيف بطريقـة العناصر المحـددة للمجـال المتـأين ثنـائي القطبيـة

زكريا الهموز* ، مازن عبد السلام* و أنور حسن مفتي**

** قسم الهندسة الكهربائية ، كلية الهندسة ، جامعة الملك فهد للبترول والمعادن*
الظهـــران – المملكة العربية السعودية

*** قسم الهندسة الكهربائية وهندسة الحاسبات ، كلية الهندسة ، جامعة الملك عبد العزيز*
جـــــدة – المملكة العربية السعودية

المستخلص . تقدم ورقة البحث طريقة تكرارية متكيفة تستخدم العناصر المحددة لتحليل المجال المتأين الناشئ حول موصلات خطوط النقل ذات التيار المستمر ثنائي القطبية والجهد العالي ، وذلك دون اللجوء إلى الاستعانة بافتراض « دويتسن » . وعلى خلاف جميع المحاولات المنشورة في أدبيات التخصص فيما يتعلق بحلول المجال المتأين ، فإن صياغة العناصر المحددة حققت تنفيذاً مباشراً للقيمة الثابتة للمجال عند سطوح الموصلات عند قيمة بداية الهالة . كذلك تأخذ ورقة البحث في الاعتبار عدم تساوي قابليتي الحركة للأيونات الموجبة والسالبة وأيضاً قيم الجهود الابتدائية .

وقد تم بناء نموذج معملي لدراسة مدى فعالية الطريقة المقترحة . وقد وجد أن خصائص الجهد – التيار المحسوبة وكذلك كثافة التيار في مستوى الأرض تتفق تماماً مع نظائرها المقاسة معملياً . وقد وجد أنه عندما تمت مراعاة عدم التساوي بين قابليتي الحركة للأيونات الموجبة والسالبة وكذلك عندما أدخلت قيم الجهود الابتدائية في الحسبان فإن النتائج التي تم التوصل إليها حسابياً تحسنت باتجاه القيم المقاسة معملياً .